Synthesis and Characterization of Manganese Ferrite Nanoparticles

A Thesis submitted

In Partial Fulfillment of the Requirements

for the degree of

MASTER OF TECHNOLOGY

in

MATERIALS & METALLURGICAL ENGINEERING

BY

ROMI BHAROL
(Roll NO. 600902010)

SCHOOL OF PHYSICS AND MATERIALS SCIENCE
THAPAR UNIVERSITY
PATIALA-147004
INDIA
July 2011

CERTIFICATE

This is to certify that the thesis entitled "Synthesis and Characterization of Manganese Ferrite Nanoparticles " submitted by Mrs. Romi Bharol is in partial fulfillment for the degree of Master Of Technology in Materials & Metallurgical Engineering embodies the work carried out by Mrs. Romi Bharol, under my supervision, in the School of Physics and Material Science Thapar University, Patiala. She has not submitted this work to any other University or Institute for the award of any degree.

Dr. S.D. Tiwari
Assistant Professor
School of Physics and Materials Science
Thapar University, Patiala

Countersigned by

Dr. O. P. Pandey
Head
School of Physics & Materials Science
Thapar University, Patiala

Dr. S. K. Mohapatra
Dean of Academic Affairs
Thapar University, Patiala

DECLARATION

I hereby declare that the thesis entitled "Synthesis and Characterization of Manganese Ferrite Nanoparticles " is the work carried out by me under the supervision of Dr. S. D. Tiwari. I have not submitted this work anywhere else for the award of any degree.

Romi

Romi Bharol

ACKNOWLEDGEMENT

First of all I express my deepest gratitude to my supervisor Dr. S. D. Tiwari for his guidance. I thank him for giving me the opportunity to work under him by putting a trust in my credentials and capabilities, and helping me in exploring my potential to the fullest.

It is pleasure to thank all my friends in our group and my lab mates who shared the moments of different tastes on different occasions. I am also thankful to Ms. Sakshi for her help during the course of thesis work.

My parents and my lovingly husband (Rajinder Singh Kaundal) have stood by me throughout this venture for which I will remain ever grateful. Their constant encouragement and support enabled me to pursue my goal easily.

Above all, words cannot express my sincere thanks to the almighty for showering countless blessings to me.

Romi Bharol

ABSTRACT

$MnFe_2O_4$ nanoparticles, having average crystallite size of about 8 nm, are synthesized with the help of co-precipitation method and are characterized by x-ray diffraction, transmission electron microscope and vibrating sample magnetometer. The Curie temperature of the system is found to be about 295 ^{0}C.

CONTENTS

LIST OF FIGURES

CHAPTER 1
INTRODUCTION

1.1 Magnetism

On the basis of alignment of magnetic dipole moments of molecules or atoms under the effect of external magnetic field the materials are classified into five main categories as diamagnetic, paramagnetic, ferromagnetic, ferimagnetic and antiferromagnetic [1-4]. Diamagnetism, paramagnetism and antiferromagnetism are weak effects on the other hand ferromagnetism and ferrimagnetism are strong effects.

1.1.1 Diamagnetism

Diamagnetism effect is observed in those materials in which atoms or molecules contain even number of electrons. In the absence of external magnetic field net magnetic dipole moment of each molecule is zero. On the application of external magnetic field atomic dipoles do not experience the torque but electronic motion within each atom is modified. Those electrons, whose current loop is so oriented that its magnetic field is in a direction similar to external field gets slow down, while those whose loops are so oriented that their own magnetic field is opposite to external magnetic field, gets accelerated. Therefore every electron pair with in same orbit acquires a net magnetic dipole moment in a direction opposite to external magnetic field [2].

1.1.2 Paramagnetism

Paramagnetism effect is observed in those materials in which atoms or molecules contain odd number of electrons. In paramagnetic materials the dipole moment of all electrons except the last unpaired electron cancels each other. Due to last unpaired electron, the magnetic moment of each atom or molecule is non zero even in the absence of external magnetic field. But due to thermal agitations at room temperature the dipoles of paramagnetic material are randomly oriented resulting in the overall dipole moment to be zero. On the application of external magnetic field each dipole experiences torque which aligns the dipole in the direction of external magnetic field resulting in finite dipole moment in the direction of external field [3].

1.1.3 Ferromagnetism

Ferromagnetic materials under the effect of external magnetic field are strongly magnetized in the direction of the field. In case of ferromagnetic materials the atomic dipoles occur in groups known as domains. In the absence of external magnetic field the dipole moments of the domains are randomly oriented resulting in zero value of net dipole moment. On the application of external magnetic field favorably oriented domains grow in size and unfavorably oriented domains reduce in size resulting in the attainment of net magnetic dipole moment in the direction of the external field [3].

1.1.4 Antiferromagnetism

In Anti-ferromagnetism the spontaneous magnetization of a unit cell is due to two interpenetrating sublattices. The spontaneous magnetization of one sublattice is equal and opposite to the other. The net dipole moment or magnetization of antiferromagnetic material is zero in the absence of external magnetic field. On the application of external magnetic field a small magnetization in the direction of external field is produced which increases with increase in temperature. At a particular temperature known as Neel temperature the magnetization is maximum and with further increase in temperature the magnetization starts decreasing. Above the Neel temperature the antiferromagnetic material becomes paramagnetic in nature [3].

1.1.5 Ferrimagnetism

Ferrimagnetisms can be considered as a special case of Anti-ferromagnetism. In this case the spontaneous magnetization of one sublattice is different from the other sublattice resulting in non zero magnetization of the unit cell. The most well known ferrite is the oxide magnetite, or Fe_3O_4, also known as lodestone. This oxide has an inverted spinel structure generally described as an FCC lattice of O^{2-} ions that form cages surrounding interstitial sites. Spinels are also viewed as having an admixture of rocksalt and zinc blende packing. Figure 1.1 and 1.2 illustrates the structure of normal and inverted spinel structure of ferrites. In the indicated cubic cell, one-eighth the size of the normal unit cell, there are eight tetrahedral sites. One of these is occupied by a Fe^{3+} ion with a spin pointing downward. Two of four octahedral sites in the cell are also occupied, one by an Fe^{3+} ion and one by an Fe^{2+} ion, both with upward spin. Thus, the compound can be written as $Fe^{2+}Fe_2{}^{3+}O_4$ in this octant cell, or $(Fe^{2+}Fe_2{}^{3+}O_4)_8$ in the normal cell. Other

magnetic ferrites have inverted spinel structures in which the magnetic moment may be viewed as deriving solely from the divalent cation. The Fe^{3+} ions on tetrahedral and octahedral sites couple anti-ferromagnetically, resulting in a cancellation of the moment from this source. A rich variety of ferrite alloys having the general formula $Me^{2+}Fe_2^{3+}O_4$, where Me^{2+} is a divalent metal ion that substitutes for Fe^{2+} (e.g., Ni^{2+}, Co^{2+}, Zn^{2+}), is possible [4]. For example, in $Co^{2+}Fe_2^{3+}O_4$, a mole of CoO is alloyed with one of Fe_2O_3. The subunit cell magnetization depends only on the Co^{2+} ion moment of $3\mu_B$. Because of moment cancellation in adjacent sublattices, the saturation magnetization of ferrites is generally less than that of metal magnets.

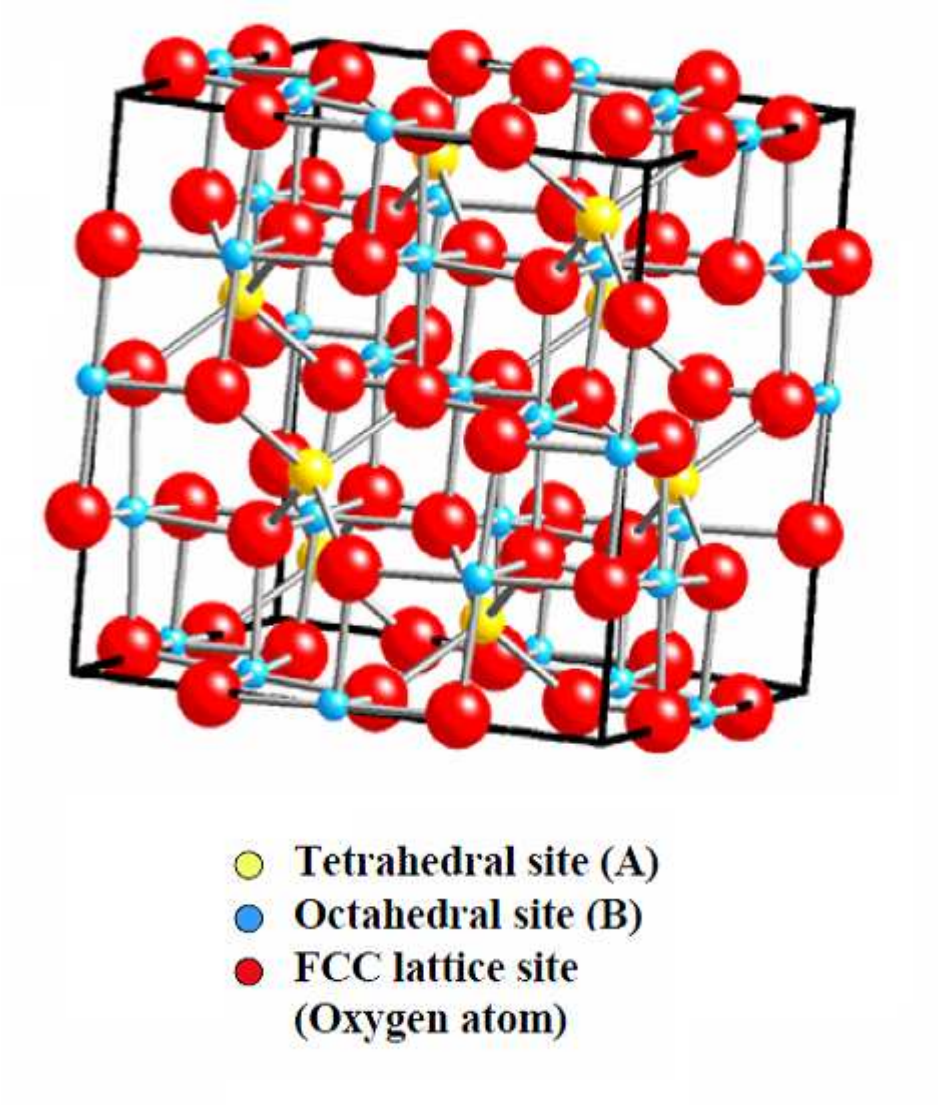

Figure 1.1: Normal Spinel structure. All divalent ions are on tetrahedral sites & trivalent ions are on octahedral sites e.g. $Zn^{2+}Fe_2^{3+}O_4$ [5].

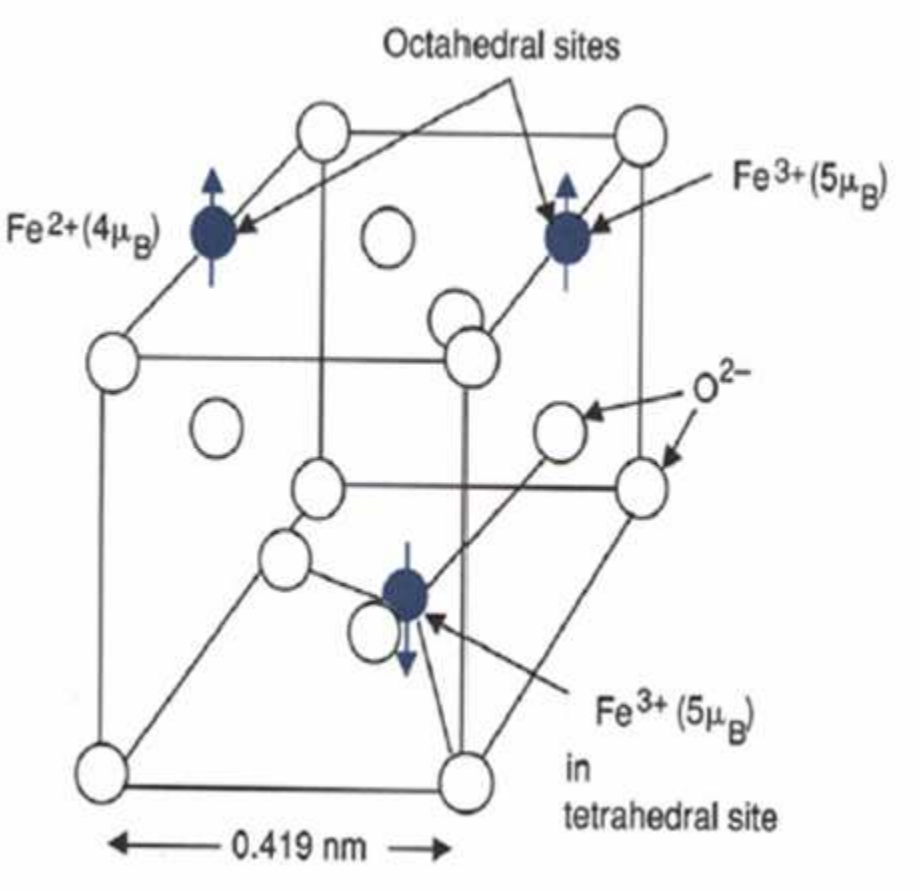

Figure 1.2: The inverse spinal structure of ferrite of the type $MeFe_2O_4$, emphasizing the magnetization of ions in octahedral and tetrahedral sites within one octant of the normal unit cell [6].

Hexagonal ferrites are an important class of magnetic ferrites that have a complex hexagonal structure similar to that of the mineral magnetoplumbite. These ferrites have the formula $MO.6Fe_2O_3$ or $MFe_{12}O_{19}$, where M is Ba, Sr, or Pb. Per formula unit, the 12 Fe^{3+} ions are arranged on several different sites as follows: 2 Fe^{3+} ions are in tetrahedral sites with spin up; 2 Fe^{3+} ions are in octahedral sites with spin up; 7 Fe^{3+} ions are in octahedral sites with spin down; 1 Fe^{3+} ion is in fivefold coordination with spin down. Thus there are four uncompensated Fe^{3+} ion moments each of magnitude$5\mu_B$. Therefore, the net formula moment is $4 \times 5\mu_B = 20\ \mu_B$. The hexagonal ferrites are used to make permanent magnets.

1.2 Magnetic Anisotropy

The theory of Ferro- and ferrimagnetisms is based on electronic exchange forces. These forces are so strong that these materials are spontaneously magnetized, even in the absence of an applied field. Yet, in the laboratory we need to apply magnetic fields to saturate a Ferro- or Ferrimagnetic material. In some cases, the material in bulk form has a remanence of nearly zero. The ferromagnets are subdivided into many small subvolumes, called domains. Each domain is spontaneously magnetized to saturation, but the direction of magnetization varies from domain to domain. The net vector sum of all the domains therefore produces a total magnetization of near zero. There are few facts about the influence of the crystal structure and the shape of grains on the direction of magnetization. The dependence of magnetic properties on a preferred direction is called magnetic anisotropy. There are several different types of anisotropy. These types are magnetocrystalline, shape and stress anisotropy.

Magnetic anisotropy strongly affects the shape of hysteresis loops and controls the coercivity and remanence. Anisotropy is also of considerable practical importance because it is exploited in the design of most magnetic materials of commercial importance.

1.2.1 Magnetocrystalline Anisotropy

Magnetocrystalline anisotropy is an intrinsic property of a ferro or ferrimagnet, independent of grain size and shape. It can be most easily seen by measuring magnetization curves along different crystal directions [7].

For example, here are magnetization curves for magnetite. Depending on the crystallographic orientation of the sample in the magnetic field, the magnetization reaches saturation in different fields.

In magnetite, above 130 K, <111> is the easy direction of magnetization, <100> is the hard direction of magnetization and <110> is the intermediate direction of magnetization. For a sphere of magnetite there will be six easy directions of magnetization corresponding to the three [111] axes.

Magnetocrystalline anisotropy is the energy necessary to deflect the magnetic moment in a single crystal from the easy to the hard direction. The easy and hard directions arise from the interaction of the spin magnetic moment with the crystal lattice.

In cubic crystals, like magnetite, the magnetocrystalline anisotropy energy is given by a series expansion in terms of the angles between the direction of magnetization and the cube axes. It is sufficient to represent the anisotropy energy in an arbitrary direction by just the first two terms in the series expansion. These two terms each have an empirical constant associated with them called the first- and second order anisotropy constants, or K_1 and K_2, respectively. At 300 K, $K_1 = -1.35 \times 10^5$ erg/cm^3 and $K_2 = -0.44 \times 10^5$ erg/cm^3.

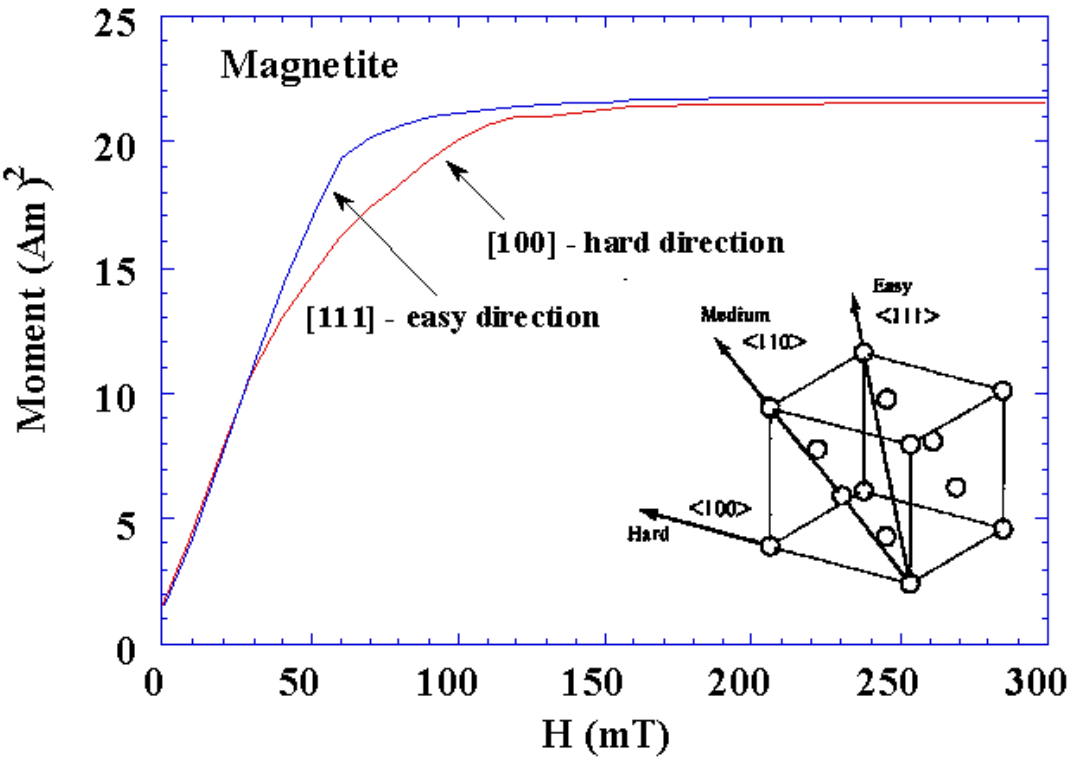

Figure 1.3: Magnetic moment vs. H curve for magnetite. Directions for easy and hard magnetizations are also shown [8].

In hexagonal crystals, like hematite, the weak ferromagnetism lies in the basal plane, which is an easy plane of magnetization. The c-axis is the hard direction. It is extremely difficult to flip the magnetization out of the basal plan into the direction of the c-axis.

1.2.2 Stress Anisotropy

In addition to magnetocrystalline anisotropy, there is another effect related to spin-orbit coupling called magnetostriction. Magnetostriction arises from the strain dependence of the anisotropy constants [9]. Upon magnetization, a previously demagnetized crystal experiences a strain that can be measured as a function of applied field along the

principal crystallographic axes. A magnetic material will therefore change its dimension when magnetized.

The inverse effect or the change of magnetization with stress also occurs. A uniaxial stress can produce a unique easy axis of magnetization if the stress is sufficient to overcome all other anisotropies. The magnitude of the stress anisotropy is described by two more empirical constants known as the magnetostriction constants and the level of stress.

1.2.3 Shape Anisotropy

The third type of anisotropy is due to the shape of a grain. A magnetized body will produce magnetic charges or poles at the surface [9]. This surface charge distribution, acting in isolation, is itself another source of a magnetic field, called the demagnetizing field. It is called the demagnetizing field because it acts in opposition to the magnetization that has produced it.

For example, take a long thin needle shaped grain. The demagnetizing field will be less if the magnetization is along the long axis than if is along one of the short axes. This produces an easy axis of magnetization along the long axis. A sphere, on the other hand, has no shape anisotropy. The magnitude of shape anisotropy is dependent on the saturation magnetization. For magnetite, smaller than about 20 microns, shape anisotropy is the dominant form of anisotropy. In larger sized particles, shape anisotropy is less important than magnetocrystalline anisotropy. For hematite, because the saturation magnetization is so low, shape anisotropy is usually never important.

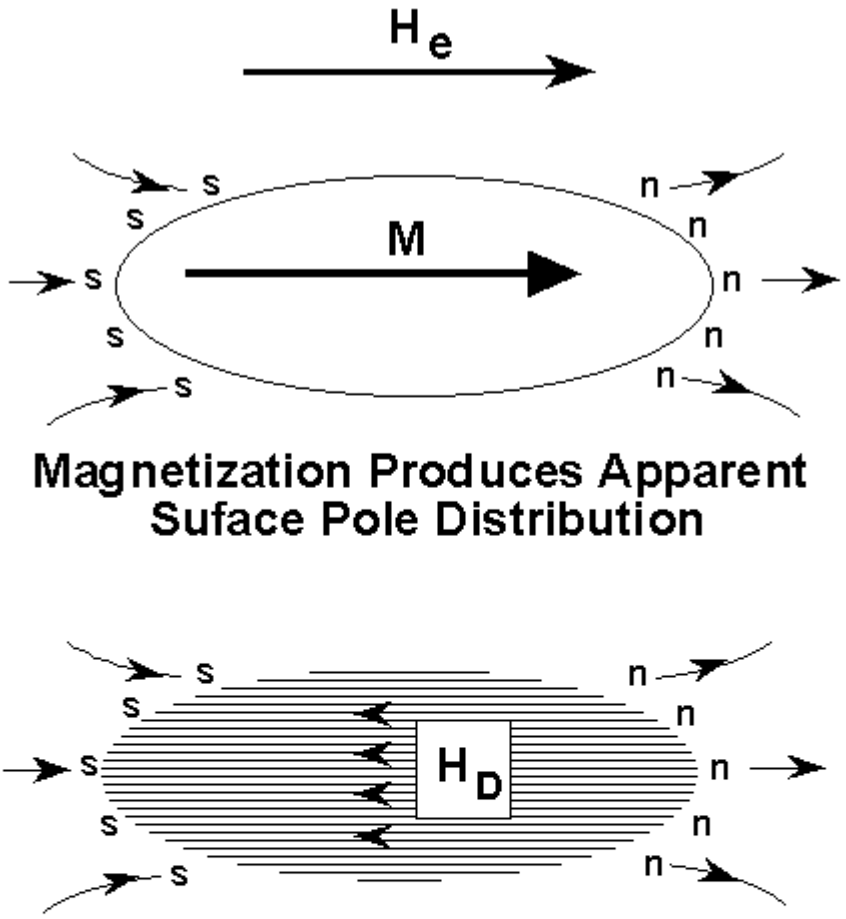

Figure 1.4: Shape anisotropy [9].

1.3 Superparamagnetism

The phenomenon by which magnetic materials show a behavior similar to paramagnetism even at temperatures lower than the Curie or the Neel temperature is known as Superparamagnetism. Superparamagnetism is a small length-scale phenomenon, where the energy required to change the direction of the magnetic moment of a particle is comparable to the ambient thermal energy. At small-length scale point, the rate at which the particles will randomly reverse direction often becomes significant. Normally, coupling forces in ferromagnetic materials cause the magnetic moments of neighboring atoms to align, resulting in very large internal magnetic fields. This effect distinguishes ferromagnetic materials from paramagnetic materials. At temperatures above the Curie temperature (or the Neel temperature for antiferromagnetic materials), the thermal energy is sufficient to overcome the coupling forces, causing the atomic magnetic moments to fluctuate randomly. Because there is no longer any magnetic order, the internal magnetic field no longer exists and the material exhibits paramagnetic behavior. If the material is non-homogeneous, one can observe a mixture of ferromagnetic and paramagnetic clusters of atoms at the same temperature, i.e. superparamagnetic stage. Superparamagnetism occurs when the material is composed of very small crystallites. In this case when the temperature is below the Curie or Neel temperature the thermal energy is not sufficient to overcome the coupling forces between neighboring atoms. The thermal energy is sufficient to change the direction of magnetization of the entire crystallite. The resulting fluctuations in the direction of magnetization cause the magnetic field to average to zero. Thus the material behaves in a manner similar to paramagnetism, except that instead of each individual atom being independently influenced by an external magnetic field, the magnetic moment of the entire crystallite tends to align with the magnetic field. The energy required to change the direction of magnetization of a crystallite is called the crystalline anisotropy energy and depends both on the material properties and the crystallite size. As the crystallite size decreases, so does the crystalline anisotropy energy, resulting in a decrease in the temperature at which the material becomes superparamagnetic. The rate at which particles will lose their direction is governed by the Neel-Arrhenius equation. It is a function of the exponential of the grain volume.

$\tau_N = \tau_0 \exp(KV/K_BT)$

where τ_N is the average length of time that it takes for the nanoparticle's magnetization to randomly flip as a result of thermal fluctuations, τ_0 is a length of time, characteristic of the material, called the attempt time or attempt period, K is the nanoparticle's magnetic anisotropy energy density and V its volume. KV is therefore the energy barrier associated with the magnetization moving from its initial easy axis direction, through a "hard plane", to the other easy axis direction and k_B is the Boltzmann constant, T is the temperature.

1.4 Literature Review and Aim of the Thesis

Magnetic oxide nanoparticles are found to exist in a rich variety of structures and chemistries and are found commonly in both terrestrial and extraterrestrial environments [10]. Magnetic nano sized ferrite particles are used extensively in many applications for example, magnetic recording media, ferrofluids and radar absorbing coatings, radio frequency coil fabrication, transformer cores, rod antennas and many branches of telecommunication and electronic engineering [11-19]. Also an extensive investigation is continuing on soft magnetic materials for their uses mainly in microwave devices. Due to their wide existence and manifold applications magnetic oxide nanoparticles have drawn considerable attention of many researchers in the past few years. Many researchers have undertaken the studies regarding size dependence of the physical and magnetic properties of Mn ferrite nanoparticles [20-28]. In order to understand their unique properties and

further promote their utility, one must fully understand the correlation between chemistry, structure, particle size, and processing [29-31].

There are several methods for the preparation of ferrite nanoparticles [32]. Out of these methods chemical precipitation and coprecipitation are the economical routes for the production of large quantities of nanosized ferrite particles [33-34]. Many other techniques for example, as sol-gel, mechanochemical processing, microemulsion and other physical methods have also used to prepare these particles [35-37]. Chemical precipitation methods have long been used for the preparation of magnetic nanoparticles, as the control over the particle size and shape can lead to the production of materials with desired magnetic properties [38]. These methods offer many advantages over other methods, such as freedom from contamination, more homogeneous mixing of the components and control over the particle size of the powders [38]. Many authors have investigated the formation of spinel ferrites from a mixture of hydroxides precipitated from a solution of the appropriate cations [38]. In this work a coprecipitation technique is used to prepare a single-phase nano-sized Mn ferrite powder.

A very important step in this process is to maintain the stoichiometry of Mn^{2+} and Fe^{3+} ions in the solution. For the synthesis of $MnFe_2O_4$ nanoparticles the ratio of Mn^{2+} and Fe^{3+} ions in the starting solution should be 1 : 2. Any departure from this ratio will lead to formation of either $Mn(OH)_2$ or $Fe(OH)_3$. This situation must be avoided. Salts of Mn^{2+} and Fe^{3+} are hydroscopic in nature and absorb water from atmosphere. Because of this reason it is difficult to maintain the required stoichiometry of ions in the solution. This motivated me to work on the synthesis of $MnFe_2O_4$ nanoparticles.

CHAPTER 2

EXPERIMENTAL TECHNIQUES

2.1 X-Ray diffractometer

X-rays are electromagnetic radiation of wavelength about 1 Å (10^{-10} m) which occur in electromagnetic spectrum between gamma-rays and the ultraviolet rays [39]. X-ray diffraction is one of the most important characterization tools used in solid state chemistry and materials science. X-ray diffraction (XRD) is a versatile and non-destructive technique which can be used to reveal the detailed information regarding chemical composition as well as crystallographic structure of natural and manufactured materials. Further X-rays enables the scientists and technologists to probe crystalline structure at the atomic level [40]. The X -ray diffraction experiment requires an X-ray source, the sample under investigation and a detector to pick up the diffracted X-rays. Figure 2.1 shows a schematic diagram of a powder X-ray diffractometer. The X-ray radiation most commonly used is that emitted by copper, whose

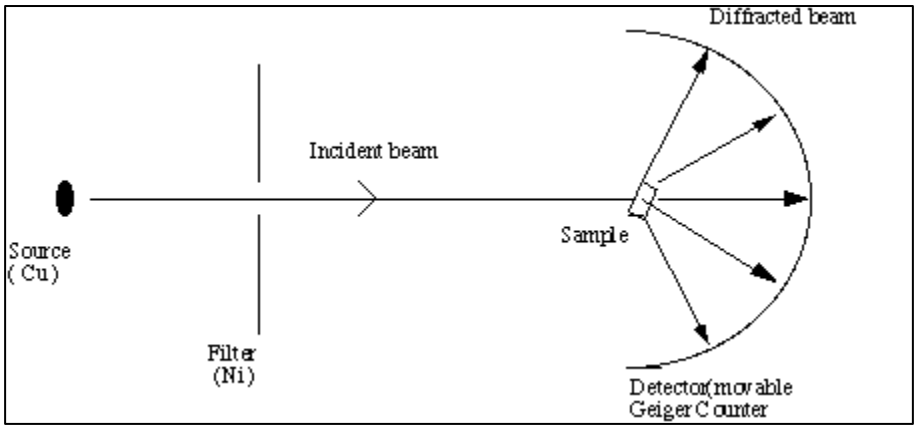

Figure 2.1: Schematic presentation of a powder X-ray diffractometer [41].

characteristic wavelength for the K_α radiation is =1.5418Å. When the incident beam strikes a powder sample, diffraction occurs in every possible orientation of 2θ. The diffracted beam may be detected by using a moveable detector such as a Geiger counter. In normal use, the counter is set to scan over a range of 2θ values at a constant angular velocity. Figure 2.2 shows the x-ray diffraction pattern from a set of parallel atomic planes.

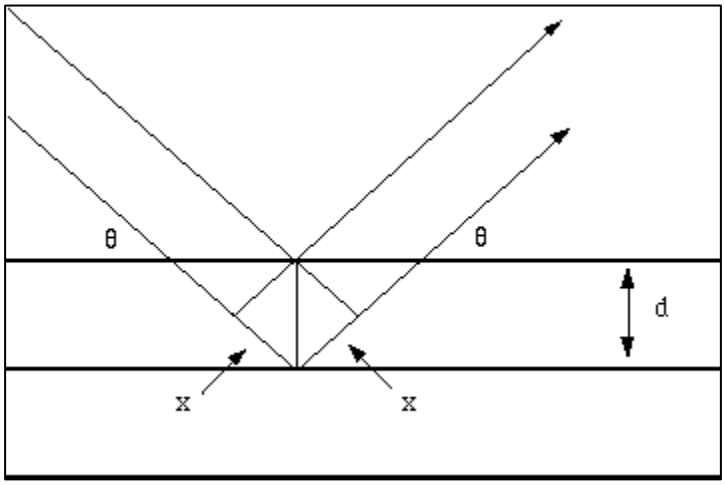

Figure 2.2: Schematic presentation of X-ray diffraction pattern from a crystal [42].

The path difference between two waves is 2d sinθ. For constructive interference between these waves, the path difference must be an integral number of wavelengths i.e.

$2d \sin\theta = n \lambda$

This is Bragg's law. With the help of this relation the possible values of d can be calculated.

2.2 Vibrating sample magnetometer

Vibrating sample magnetometer (VSM) is used to study the magnetic behavior of magnetic materials. VSM operates on Faraday's Law of Induction, which tells us that a changing magnetic field will produce an electric field. This electric field can be measured and can tell us information about the changing magnetic field [43]. A VSM operates by first placing the sample to be studied in a constant magnetic field. If the sample is magnetic, this constant magnetic field will magnetize the sample by aligning the magnetic domains, or the individual magnetic spins, with the field. The stronger the constant field, the larger the magnetization will be. The magnetic dipole moment of the sample will create a magnetic field around the sample, sometimes called the magnetic stray field. As the sample is moved up and down, this magnetic stray field changes as a function of time and can be sensed by a set of pick-up coils. The alternating magnetic field will cause an electric field in the pick-up coils according to Faraday's Law of Induction. This current will be proportional to the magnetization of the sample. The greater the magnetization, greater is the induced current. The induction current is

amplified by an amplifier. The various components are hooked up to a computer interface.

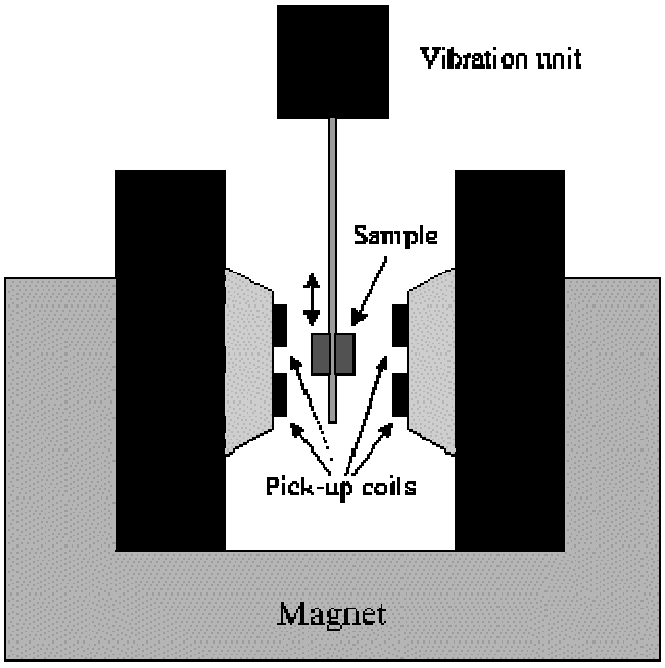

Figure 2.3: Schematic presentation of VSM [44].

2.3 Transmission Electron Microscope

Transmission electron microscope (TEM) is a microscope that allows for high resolution imaging as well as for chemical and structural studies on atomic scale [45]. An image is formed by a beam of electrons that has passed through the sample. The information like size distribution, shape and crystal structure can be obtained by using transmission electron microscopy. Transmission electron microscopy is a microscopy technique whereby a beam of electrons is transmitted through an ultra thin specimen, interacting with the specimen as it passes through. An image is formed from the interaction of the electrons transmitted through the specimen; the image is magnified and

focused onto an imaging device, such as a fluorescent screen, on a layer of photographic film, or to be detected by a sensor such as a CCD camera.TEMs are capable of imaging at a significantly higher resolution than light microscopes, owing to the small de Broglie wavelength of electrons. This enables the instrument's user to examine fine detail—even as small as a single column of atoms, which is tens of thousands times smaller than the smallest resolvable object in a light microscope. TEM forms a major analysis method in a range of scientific fields, in both physical and biological sciences. TEMs find application in materials science as well as in nanotechnology. At smaller magnifications TEM image contrast is due to absorption of electrons in the material, due to the thickness and composition of the material. At higher magnifications complex wave interactions modulate the intensity of the image, requiring expert analysis of observed images. Alternate modes of use allow for the TEM to observe modulations in chemical identity, crystal orientation, electronic structure and sample induced electron phase shift as well as the regular absorption based imaging. The ray diagram for the transmission electron microscope is shown in figure 2.4. Electron gun is used to emit a beam of electrons. This beam of electrons is accelerated by using electric filed. Magnetic field and electric field control the path of electrons. Electron wavelength of the order of $2x10^{-12}$ m and normal resolution of the order of 2Å is achieved.

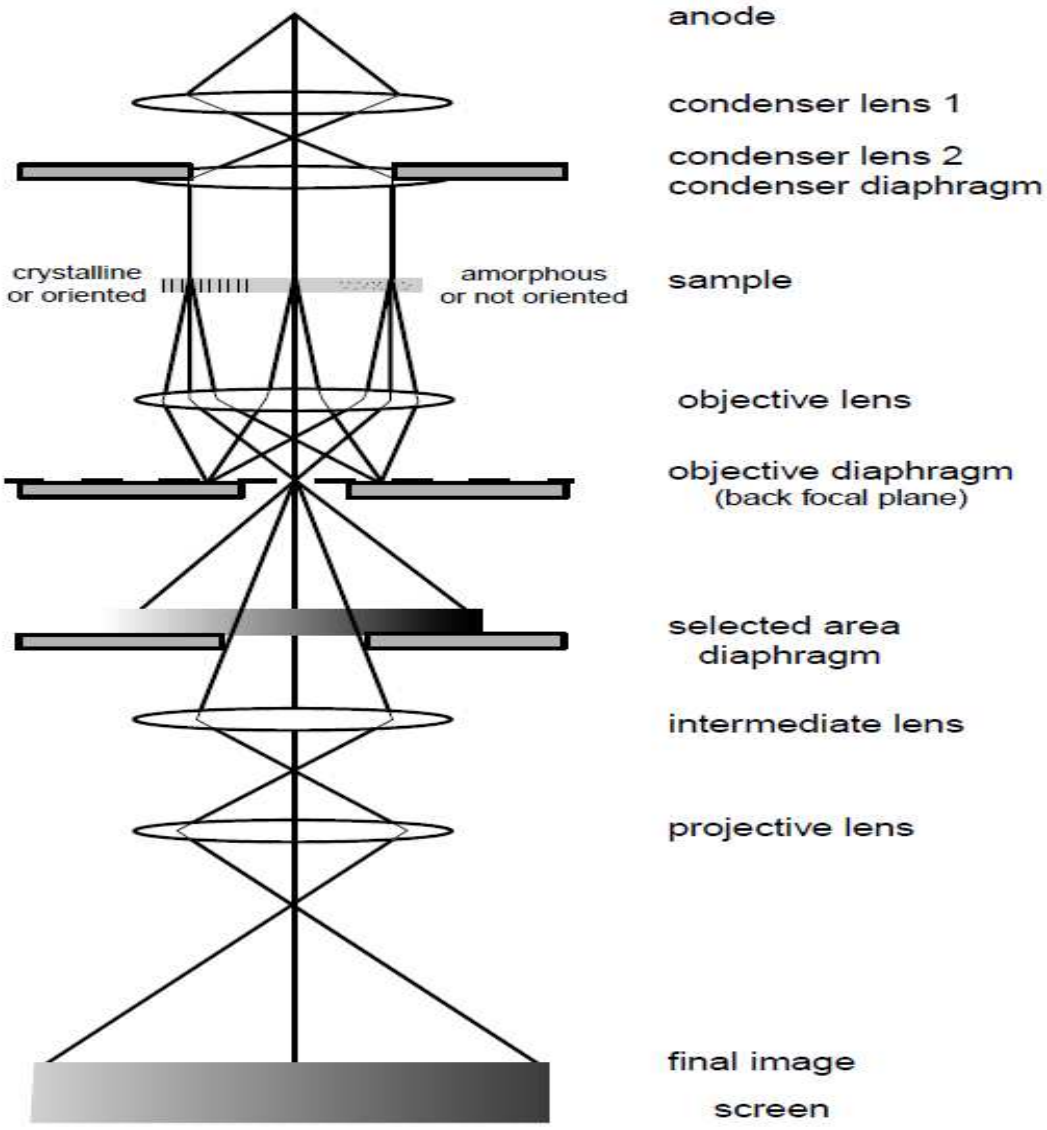

Figure 2.4: Ray diagram for a transmission electron microscope in image mode. In diffraction mode, an other intermediate lens is inserted to image on the screen the diffraction pattern of the back focal plane [46].

CHAPTER 3

SYNTHESIS, RESULTS AND DISCUSSION

3.1 Synthesis

There are many physical and chemical methods for the preparation of nanoparticles of any material. Usually chemical methods are better than physical methods because chemical reaction take place at atomic/molecular level so particle shape, size and morphology can be controlled in a better way. Keeping this thing in mind I followed a chemical method for the synthesis of $MnFe_2O_4$ nanoparticles. In present work the nanoparticles of $MnFe_2O_4$ are synthesized by a co-precipitation method [47]. In this method $Fe^{3+}$and Mn^{2+} ions in appropriate ratio are precipitated simultaneously in an aqueous solution with the help of NaOH. In this method NaOH solution is added drop wise in a solution containing Mn^{2+} and Fe^{3+} ions in stoichiometric amount. The resulting precipitate is of $MnFe_2O_4$. A very important step in this process is to maintain the stoichiometry of Mn^{2+} and Fe^{3+} ions in the solution. In the starting solution the ratio of Mn^{2+} and Fe^{3+} ions should be 1 : 2. Any departure from this ratio will lead to formation of either $Mn(OH)_2$ or $Fe(OH)_3$. This situation must be avoided. This aim can only be achieved by preparing solutions of Mn^{2+} and Fe^{3+} ions of well known concentrations.

3.1.1 Preparation of $FeCl_3$ solution of known concentration

Approximately 0.2 M solution of $FeCl_3.6H_2O$ is prepared by dissolving 0.2 mole $FeCl_3.6H_2O$ (i.e. 108.12g) in 1000 ml solution using a volumetric flask. From the

volumetric flask, 50 ml solution is taken and diluted to 100 ml. This makes the concentration of this solution to be 0.1 M. From this diluted solution, 25 ml solution is taken in a conical flask. In this 20 ml concentrated HCl is added. The resulting solution is warmed (70-90^{0}C) and reduced with $SnCl_2$ solution and then cooled. Because of this the Fe^{3+} ions present in the solution is converted into Fe^{2+} ions. Now the concentration of ferrous ions in the solution is estimated by titration method. For this 10 ml $HgCl_2$ solution is added and then diluted to about 250 ml. After this 15 ml concentrated H_2SO_4, 5 ml of phosphoric acid and 3 drops of diphenylamine indicator are added. The final solution is titrated with standard $K_2Cr_2O_7$ solution until colour changes from green to a pale blue (violet) colour. The whole process is repeated three times. Result of this procedure gives the amount of Fe^{3+} ions in the original solution to be 0.01101 ± 0.00002 g / ml.

Reactions involving in this procedure are as follows

$$2Fe^{3+} + Sn^{2+} \rightarrow 2Fe^{2+} + Sn^{4+}$$

$$6Fe^{2+} + Cr_2O_7^{2-} + 14H^+ \rightarrow 6Fe^{3+} + 2Cr^{3+} + 7H_2O$$

3.1.2 Preparation of $MnCl_2$ solution of known concentration

The amount of manganese in a solution of manganese chloride is decided by a gravimetric method. In this method, the manganese is precipitated as ammonium manganese phosphate ($MnNH_4PO_4.H_2O$) in slightly ammonical solution containing excess of ammonium salts. After drying at 100-105 ^{0}C the precipitate is ignited and weighted as $Mn_2P_2O_7$.

Approximately 0.2 M solution of $MnCl_2.2H_2O$ is prepared by dissolving 0.1 mole (16.19 g) of $MnCl_2.2H_2O$ in 500 ml solution using a volumetric flask. 10 ml of this solution is taken in a beaker and 5 ml concentrated HCl is added. The resulting solution is diluted to 125 ml. After this the solution is almost neutralize with diluted ammonia solution. In this solution, 20 g of NH_4Cl and 2 g of $(NH_4)_2HPO_4$ are added. The solution is heated to 90-95 ^0C and diluted ammonia solution is added drop wise with constant stirring. Due to this a precipitate of $Mn_3(PO_4)_2$ is formed. This solution is kept at room temperature for 3 hours. The precipitate is washed several times with distilled water and filtered on ash less filter paper. The precipitate along with the filter paper is put inside a pre weighted alumina crucible and heated at about 750 ^0C. The resulting material is weighted as $Mn_2P_2O_7$ to constant weight.

Reactions involving in this procedure are as follows.

$$Mn^{2+} + 2NH_3 + 2H_2O \rightarrow Mn(OH)_2 + 2NH_4^+$$

$$Mn^{2+} + NH_3 + HPO_4^{2-} \rightarrow Mn(NH_4)PO_4\downarrow$$

$$3Mn^{2+} + 2HPO_4^{2-} \rightarrow Mn_3(PO_4)_2\downarrow + 2H^+$$

Procedure followed in Sections 3.1.1 and 3.1.2 is taken from Reference [48].

3.1.3 Synthesis of $MnFe_2O_4$ nanoparticles

In the present work sample of $MnFe_2O_4$ is prepared by coprecipitation method [47]. In this method NaOH solution is added drop wise in a solution containing Mn^{2+} and Fe^{3+} ions, in appropriate ratio, with constant stirring until pH of the system reaches to 12. The chemical reaction undergoing in this process is as follows.

$$Mn^{2+} + 2\ Fe^{3+} + x\ OH^- \rightarrow MnFe_2O_4 + (x-8)\ OH^- + 4\ H_2O$$

In a 250 ml beaker solutions of $FeCl_3$ and $MnCl_2$ are taken such that ratio of Mn^{2+} and Fe^{3+} ions is 1:2. In this 2 M NaOH solution is added drop wise with constant stirring until pH of the system reaches to 12. The precipitate thus formed is washed several times with distilled water and dried at 60 ^{0}C. The dried sample is grinded for further use. The x-ray diffraction pattern of the power thus prepared is shown in Figure 3.1. From this pattern it is clear that the prepared powder sample of $MnFe_2O_4$ is amorphous.

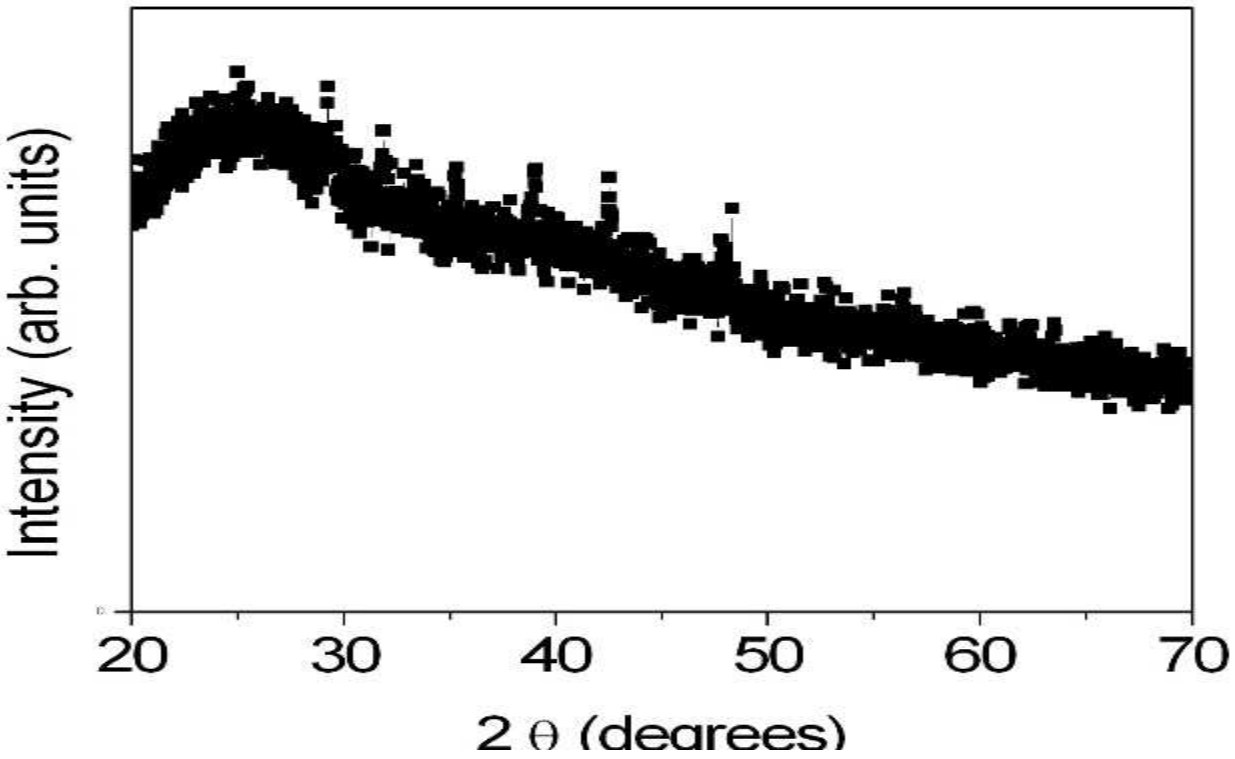

Figure 3.1: Room temperature x-ray diffraction pattern of amorphous $MnFe_2O_4$.

Another sample of $MnFe_2O_4$ is prepared following a procedure described below. In a 250 ml beaker prepared solutions of $FeCl_3$ and $MnCl_2$ are taken keeping the ratio of

Mn^{2+} and Fe^{3+} ions to be 1:2. In this 2 M NaOH solution is added drop wise with constant stirring and maintaining the temperature of the solution at 90 ^{0}C, until the pH of the system reached to 12. The resulting precipitate is kept at 90 ^{0}C for 30 minutes. After this the precipitate is allowed to cool. The resulting precipitate is washed several times with distilled water and dried at 60 ^{0}C. The material is grinded to get the powder sample. Room temperature x-ray diffraction pattern of the powder sample thus obtained is shown in figure 3.2. From this pattern it is clear that the powder sample is single phase $MnFe_2O_4$.

3.2 Structural Characterization

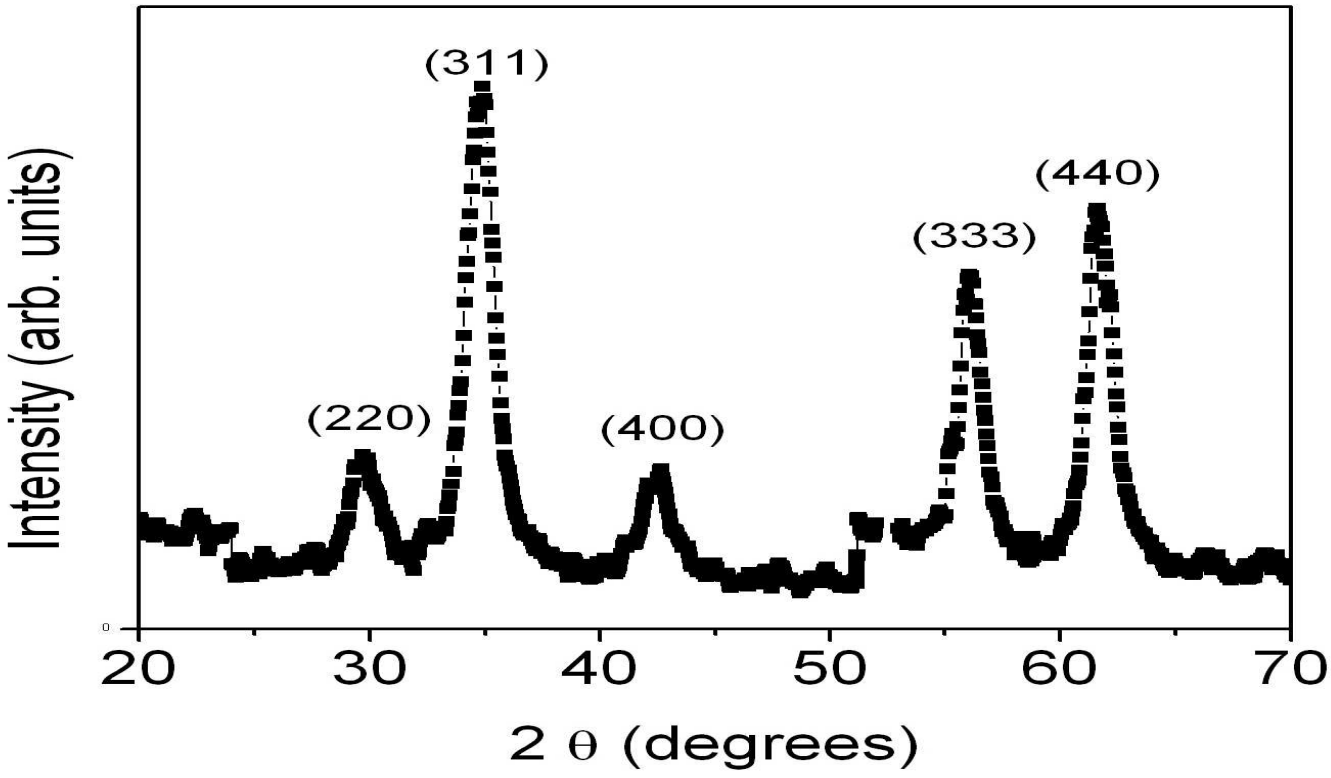

Figure 3.2: Room temperature x-ray diffraction pattern of $MnFe_2O_4$ nanoparticles.

Figure 3.2 shows room temperature x-ray diffraction pattern of the synthesized powder sample of $MnFe_2O_4$. From this pattern it is noticed that the peaks are broadened. This indicates that the sample is nanocrystalline. The average crystallite (*d*) size is calculated using the modified Scherrer formula

$$d = 0.9 \lambda / Cos\ \theta_B (B_M^2 - B_S^2)^{1/2}$$

where λ is the wavelength of the x-ray used, θ_B is the Bragg angle, B_M is the full width at half-maximum (FWHM) of a peak in radians and B_S is the FWHM of the same peak of a standard sample. Two most intense peaks in Figure 3.2 are used to calculate the average crystalline size using the modified Scherrer formula. This turns out to be about 8 nm. The use of $(B_M^2 - B_S^2)^{1/2}$ instead of B_M in the Scherrer formula takes care of instrumental broadening.

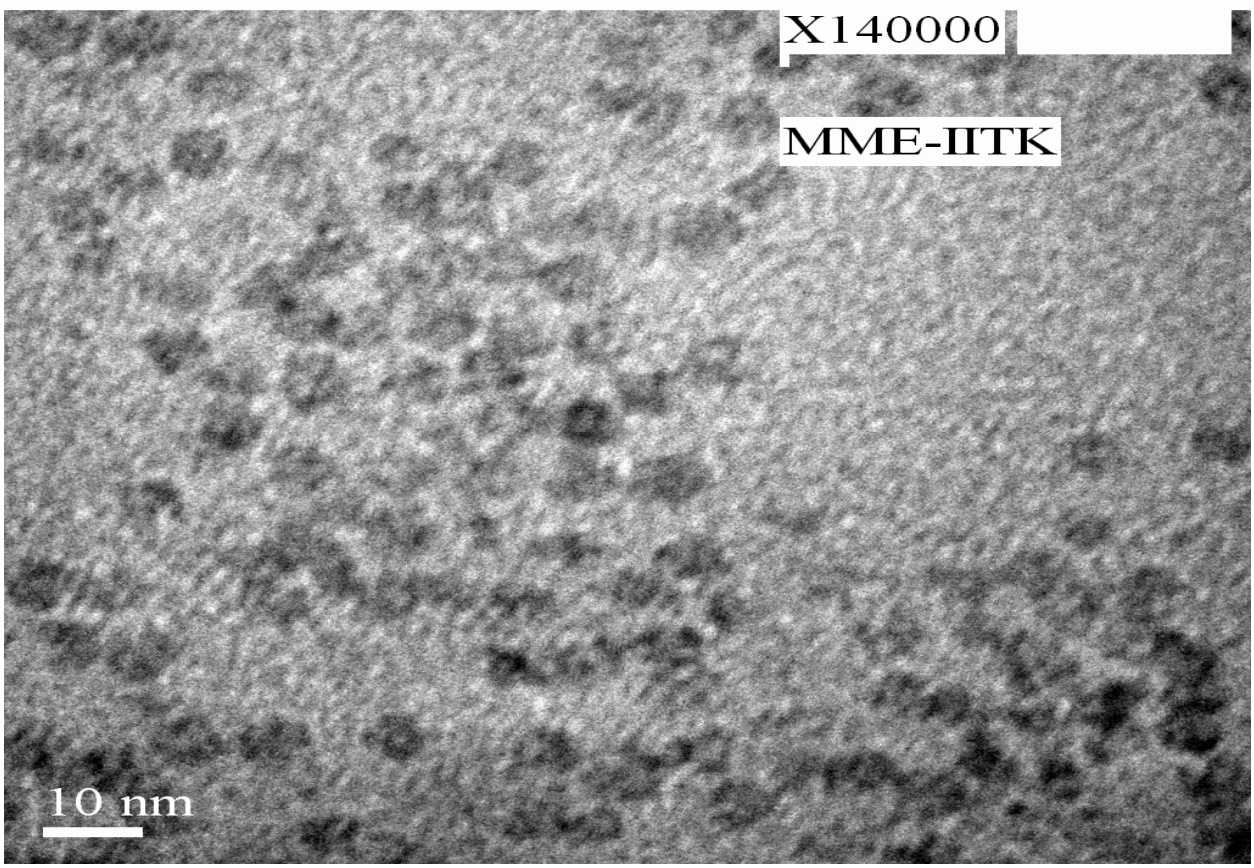

Figure 3.3: Transmission electron micrograph of $MnFe_2O_4$ nanoparticles.

The prepared sample of $MnFe_2O_4$ nanoparticles are also characterized by transmission electron microscope. For this the powder sample is dispersed in methyl alcohol and a drop of this dispersion is allowed to dry on the transmission electron microscopy grid. The micrograph thus obtained is shown in Figure 3.3. From this micrograph it is noticed that the particles are on average about 8 nm in diameter. This result is in accordance with the result obtained from x-ray diffraction.

3.3 Magnetization Measurements

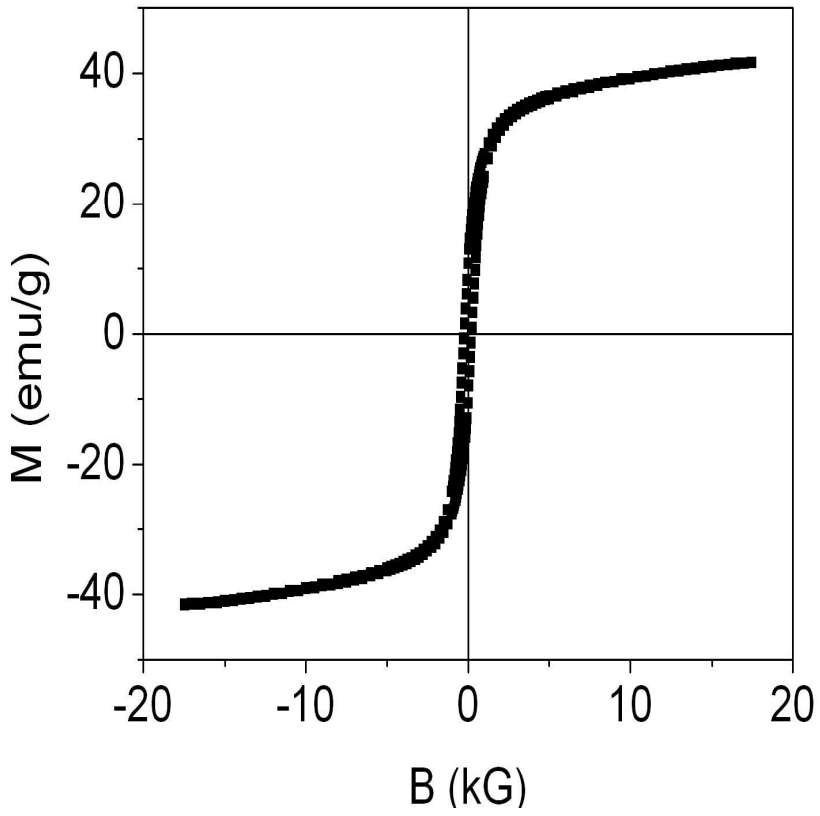

Figure 3.4: Magnetization *M* as a function of applied magnetic field *B* for $MnFe_2O_4$ nanoparticles at room temperature.

Magnetic properties of the prepared sample of $MnFe_2O_4$ nanoparticles are studied with the help of vibrating sample magnetometer. For this 20 mg of powder sample of $MnFe_2O_4$ nanoparticles is packed inside Teflon tape for the magnetization measurements. Figure 3.4 shows magnetization *M* versus applied magnetic field *B* for the $MnFe_2O_4$

nanoparticles at room temperature. This figure shows that the magnetization increases with increasing magnetic field and saturates at higher magnetic fields. From this figure it is worth noting that the coercive field and remanence magnetization is very small (approximately zero). These are characteristics of super paramagnetic particles. In higher magnetic fields all the particle magnetic moments align themselves along the applied field direction giving rise to saturation of the magnetization. From the value of saturation magnetization the average particle magnetic moment of the $MnFe_2O_4$ nanoparticles is estimated to be about 3600 Bohr magnetons.

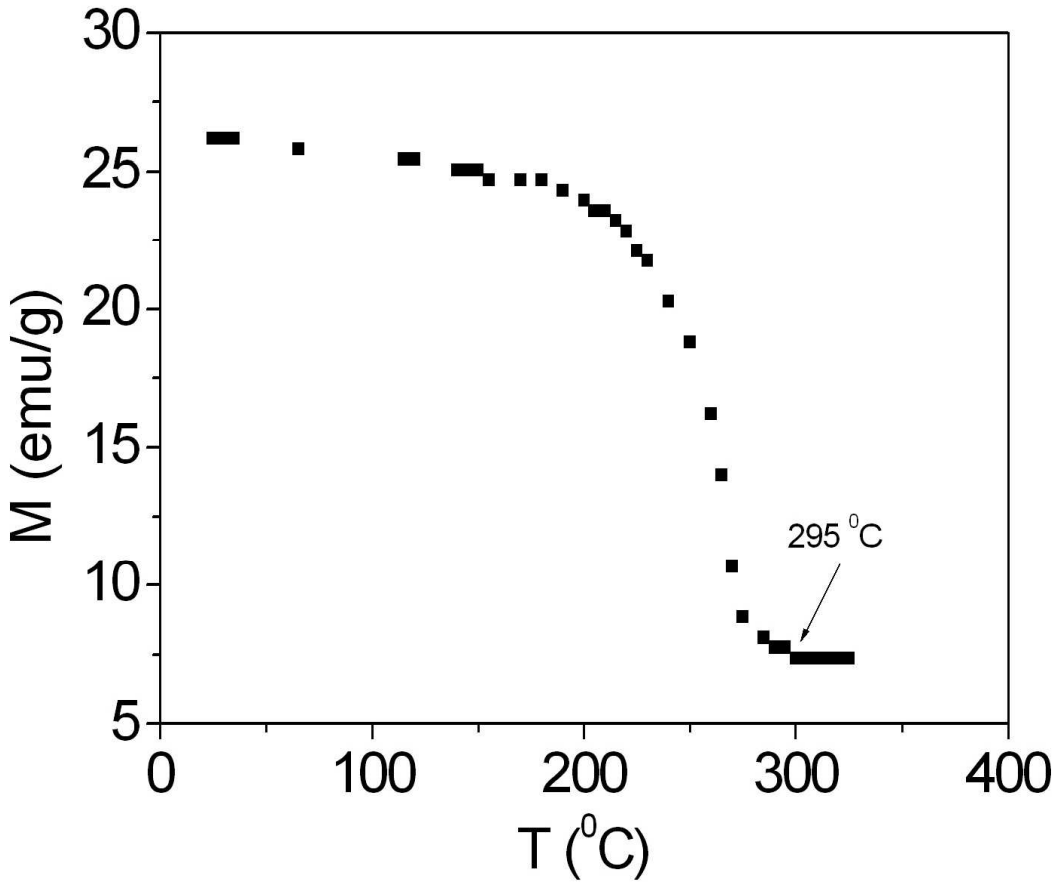

Figure 3.5: Magnetization as a function of temperature for the $MnFe_2O_4$ nanoparticles in 1000 G applied magnetic field.

Magnetization as a function of temperature measurement is also done for the $MnFe_2O_4$ nanoparticles using the vibrating sample magnetometer to determine its Curie temperature T_C. For this 20 mg of the powder sample is packed inside aluminum foil. The Magnetization *M* as a function of temperature *T* in applied magnetic field of 1000 G is shown in Figure 3.5. From this figure it is seen that the magnetization decreases slowly with increasing temperature up to 200 ^{0}C. After this the magnetization suddenly starts decreasing with increasing temperature drastically up to 295 ^{0}C. The magnetization of the system does not decrease significantly for any further increase in the temperature. This

measurement indicates that the Curie temperature T_C of the $MnFe_2O_4$ nanoparticles is about 295 ^{0}C. Value of this Curie temperature is very close to the Curie temperature of bulk $MnFe_2O_4$ reported to have a value of about 300 ^{0}C [49].

CHAPTER 4

CONCLUSIONS

In this work $MnFe_2O_4$ nanoparticles having average crystallite size of about 8 nm are synthesized with the help of coprecipitation method using $MnCl_2$ and $FeCl_3$ aqueous solutions of well known concentrations. This method prevents formation of either $Mn(OH)_2$ or $Fe(OH)_3$ along with the desired $MnFe_2O_4$ nanoparticle sample. The average crystallite size is found to be about 8 nm from the x-ray diffraction data using the modified Scherrer formula. From the transmission electron micrograph the particles are also found to be about 8 nm is size. The room temperature magnetization as a function of applied magnetic field measurement confirms the superparamagnetic nature of the sample. The Curie temperature of the nanoparticles sample is found to be close to the Curie temperature of the bulk sample.

In this work sample of $MnFe_2O_4$ nanoparticles of single average crystallite size is synthesized. In future one may synthesize $MnFe_2O_4$ nanoparticles of different sizes and may study their size dependent magnetic properties.

References

[1] W. F. Smith and J. Hashemi, *Foundation of Materials Science and Engineering* (McGraw Hill International Edition, Fourth Edition, 2006).

[2] S.O. Pillai, *Solid State Physics* (New Age Techno Press, 6th ed., 2010).

[3] C. Kittel, *Introduction to Solid State Physics* (John Wiley and Sons, 5th ed., 1976).

[4] V. Raghavan, *Materials Science and Engineering* (PHI Learning Private Limited, Fifth Edition, 2010).

[5] http://wikis.lib.ncsu.edu/index.php/Spinel

[6] F. S. James and K M. Madanapalli, *Introduction to Materials Science for Engineers* (Pearson Education, 6th ed., 2005).

[7] http://www.cwscholz.net/projects/da/node8.html

[8] B. D. Cullity and C. D. Graham, *Introduction to Magnetic Materials* (John Wiley and Sons, 2nd ed., 2009).

[9] http://www.scribd.com/doc/55725280/11/Stress-Anisotropy

[10] C Buzea, I. B. Pacheco and K Robbie, Biointerphases **2**, MR17 (2007).

[11] N. Ichnose, *Superfine Particle Technology* (Springer-Verlag, 1992).

[12] K. J. Viney and R. M. Jha, *Radar Absorbing Materials* (Kluwer Academic Publishers, 1996).

[13] T Abbas, Y Khan, M Ahmed and S Anwar, Solid State Communication **82**, 701 (1992).

[14] E. C. Snelling , Soft Ferrites, Properties and Applications(London: Butter Worth 2nd ed.1988).

[15] E. C. Snelling, Proc. of 5th Int. Conf. on Ferrites (India) 1989.

[16] M Schaefer, G Dietzmann and H Wirth, J. Magn. Magn. Mater. **101**, 95 (1991).

[17] J A T Taylor, S T Reczek and A Rosen, Am. Ceram. Soc. Bull. **74**, 91 (1995).

[18] M Rozman and M Drofenik, J. Am. Ceram. Soc. **81**, 1757 (1998).

[19] S H Chen, S C Chang and L N Lin, J. Magn. Magn. Mater. **209**, 193 (2000).

[20] Z X Tang, C M Sorensen and K J Klabunde, Phys. Rev. Lett. **67**, 3602 (1991).

[21] G U Kulkarni, K R Kannan, T Arunarkavalli and C N R Rao, Phys. Rev. B **49**, 724 (1994).

[22] J. P. Chen, C. M. Sorensen, K. J. Klabunde, G. C. Hadjipanayis, E. Devlin, and A. Kostikas, Phys. Rev. B **54**, 9288 (1996).

[23] P. J. van der Zaag, A. Noordermeer, M. T. Jonson, and P. F. Bongers, Phys. Rev. Lett. **68**, 3112 (1992).

[24] M. Muroi, R. Street, and P. G. McCormick, Phys. Rev. B **63**, 184414 (2001).

[25] L Chao and Z J Zhang, Chem. Mater. **13**, 2092 (2001).

[26] Z J Zhang, Z L Wang, B C Chakoumakos and J S Yin, J. Am. Chem. Soc. **120**, 1800 (1998).

[27] C N Chinnasamy, A Yang, S D Yoon, K Hsu, M D Shultz, E E Carpenter, S Mukerjee, C Vittoria and V G Harris , J. Appl. Phys. **101**, 09M509 (2007).

[28] Z X Tang, J P Chen, C M Sorensen, K J Klabunde and G C Hadjipanayis, Phys. Rev. Lett. **68**, 3114 (1992).

[29] M Yokoyama, T Sato and E Ohta and T. Sato, J. Appl. Phys. **80**, 1015 (1996).

[30] J Shi, S Glder, K Babcock and D D Awschalom , Science. **271**, 937 (1996).

[31] A Navrotsky, L Mazeina and J Majzlan, Science. **319**, 1635 (2008).

[32] M.A.Ahmed, N.Okasha and S.I. El-Del, Nanotechnology, **19**, 065603 (2008).

[33] D. H. Chen and X. R. He, Mater. Res. Bull., **36**, 1369 (2001).

[34] A. E. Berkowitz, J. A. Lahut, and C. E. Van Buren, IEEE Trans. Magn. **16**, 184 (1980).

[35] C. H. Peng, H. W. Wang, S. W. Kan, M. Z. Shen, Y. M. Wie, and S. Y. Chen, J. Magn. Magn. Mater. **113**, 284 (2004).

[36] J. Ding, P. G. McCormick, and R. Street, J. Magn. Magn. Mater. **171**, 309 (1997).

[37] J. Ding, X. Y. Liu, J. Wang, and Y. Shi, Mater. Lett. **19,** 44 (2000).

[38] H. Robbins, Proc. IFC, Japan, 1980.

[39] M A Ahmed, N Okasha and S I El-Dek. Preparation and characterization of nanometric Mn ferrite via different methods, Nanotechnology **19**, 065603 (2008).

[40] http://www.geosci.ipfw.edu/XRD/techniqueinformation.html

[41] Arthur Beiser, Concepts of Modern Physics (Tata McGraw-Hills, 1997).

[42] S.O.Kasap, Principles of Electronic Materials and Devices (Tata McGraw-Hill, 2007).

[43] http://en.wikipedia.org/wiki/Vibrating_sample_magnetometer

[44] http://www.el.utwente.nl/tdm/istg/research/vsm/vsm.htm

[45] http://en.wikipedia.org/wiki/Transmission_electron_microscopy

[46] http://cimewww.epfl.ch/people/cayron/Fichiers/thesebook-chap3.pdf

[47] R. V. Upadhyay, K. Parekh, and R. V. Mehta, Phys. Rev. B **68**, 224434 (2003).

[48] Vogel's textbook of quantitative chemical analysis (5^{th} ed.; revised by G. H. Jeffery et al., Longman Scientific and Technical, 1989).

[49] Z. X. Tang, C. M. Sorensen, K. J. Kaubunde, and G. C. Hadjipanayis, Phys. Rev. Lett. **67**, 3602 (1991).